1. Introduction

Chronic hepatitis C virus (HCV) infection causes progressive liver inflammation, which predisposes patients to possible liver cirrhosis and, finally hepatocellular carcinoma (HCC) [1,2]. Antiviral therapy for chronic HCV infection comprises interferon (IFN), pegylated interferon plus ribavirin (PegIFN/RBV), or a combination of PegIFN/RBV and a HCV-related protease inhibitor. Patients who achieve a sustained virological response (SVR) with successful eradication of HCV, or even those with a non-virological response (NVR) but showing improvement of liver inflammation or the serum alanine aminotransferase (ALT) level have a reduced risk of progression to HCC [3–6]. A meta-analysis of randomized controlled trials suggests that IFN therapy can efficiently reduce HCC development in patients with HCV-related cirrhosis [7].

The oxidative stress induced by reactive oxygen species (ROS) has a close association with the inflammatory process in hepatitis [8,9]. Healthy individuals have protective mechanisms against oxidative stress, i.e., induction of anti-oxidative substrates such as glutathione, thioredoxin, vitamin A and vitamin E, or enzymes for removing ROS such as superoxide dismutase, catalase and glutathione peroxidase. However, in patients of chronic hepatitis C, these protective mechanisms are impaired, and the resulting long-term exposure to oxidative stress during viral infection leads to progressive hepatitis accompanied by a risk of HCC [10–12].

Metabolome analysis has emerged as a powerful technique for detecting low-molecular-weight metabolites in cells. Metabolome profiling approaches based on capillary electrophoresis–time-of-flight mass spectrometry (CE-TOFMS) have led to the discovery of ophthalmate (γ-glutamyl-2-aminobutyrylglycine) as a biomarker of reduced glutathione depletion in mice with acetaminophen-induced hepatotoxicity [13,14]. Recently, the serum metabolites in a total of 248 samples from patients with nine types of liver disease were analyzed comprehensively using this approach, and increased levels of γ-glutamyl dipeptides in the majority were reported [15]. That study demonstrated that γ-glutamyl dipeptides are synthesized via ligation of glutamine with various amino acids and amines by γ-glutamylcysteine synthetase, which is under feedback inhibition by glutathione, and that the level of γ-glutamyl dipeptides represents the degree of glutathione production. Therefore, γ-glutamyl dipeptides are likely to be key metabolites reflecting the extent of liver tissue injury due to oxidative stress, suggesting that monitoring of their levels in serum may be useful for predicting the course of liver disease in patients with HCV infection. In addition, γ-glutamyl transferase (GGT) is the enzyme responsible for the extracellular catabolism of glutathione, and a recognized source of γ-glutamyl dipeptides. Thus GGT can be used as a marker to indicate the amelioration of oxidative stress [16].

The metabolism of human liver cells under conditions of HCV-related hepatitis has not been extensively investigated. In addition, the changes in serum metabolite levels in patients with chronic hepatitis C treated with PegIFN/RBV remain unknown. Such analysis would yield a considerable amount of useful information on the metabolism of these patients, and might lead to the discovery of new biomarkers of chronic hepatitis C that could be useful in clinical practice. In the present study, we used CE-TOFMS to analyze serum samples collected from patients with chronic HCV infection before and after PegIFN/RBV therapy.

2. Materials and methods

2.1. *Patients and details of PegIFN/RBV therapy*

Twenty patients who received PegIFN/RBV combination therapy for chronic hepatitis C were enrolled. These patients comprised 6 men and 14 women, with an age range of 38 to 70 years (52.8 ± 9.6 years, mean ± standard deviation). All of the patients had HCV genotype 1b infection with a high viral load exceeding 5 logIU/ml. Patients with alcoholic liver injury, autoimmune liver disease, and those positive for hepatitis B surface antigen were excluded. All patients were treated with a combination of PegIFN-alpha 2b (Pegintron; MSD K.K., Tokyo, Japan) and RBV (Rebetol; MSD K.K.) in accordance with the Japanese standard prescription information supplied by the Japanese Ministry of Health, Labour and Welfare. Briefly, PegIFN was administered subcutaneously once a week and RBV was given orally twice a day to achieve the total dose. The dosages of pegIFN and RBV were determined on the basis of body weight. Patients with body weights of 35–45, 46–60, 61–75, and 76–90 kg were given PegIFN at doses of 60, 80, 100, and 120 μg, respectively, and those with body weights of <60, 60–80, and >80 kg were given RBV at doses of 600, 800, and 1000 mg, respectively. Virological responses were evaluated at 24 weeks after completion of treatment, and the clinical outcome was classified as either an SVR with HCV eradication, or an NVR without HCV eradication. Patients were considered to have achieved an SVR if monitoring at four-week intervals confirmed negativity for HCV RNA for 24 weeks after completion of the therapy. Virological responses were assayed on the basis of serum HCV RNA using a real-time PCR assay kit (COBAS TaqMan HCV Auto, Roche Diagnostics). Single nucleotide polymorphism of interleukin (IL) 28B (rs8099917) was determined by direct sequencing of genomic DNA from patients, and classified into two types: the major homozygote (T/T: homozygosity for the major allele), and the minor heterozygote or homozygote (T/G or G/G: heterozygosity or homozygosity for the minor allele).

2.2. *CE-TOFMS technique for profiling of serum metabolites*

In all CE-TOFMS experiments, we used an Agilent CE capillary electrophoresis system (Agilent Technologies, Waldbronn, Germany), an Agilent G3250AA LC/MSD TOF system (Agilent Technologies, Palo Alto, CA), an Agilent 1100 series binary HPLC pump, a G1603A Agilent CE-MS adapter and a G1607A Agilent CE-ESI-MS sprayer kit. Data were acquired with the G2201AA Agilent ChemStation software for CE and Analyst QS in the Agilent TOFMS software.

The metabolites were separated in a fused silica capillary (50 μm i.d. × 100 cm) filled with 1 mol/L formic acid as the electrolyte [13]. A sample solution was injected at 50 mbar for

3 s (3 nL) and a voltage of 30 kV was applied. The capillary temperature and sample tray were set at 20 °C and below 5 °C, respectively. Methanol/water (50% v/v) containing 0.1 μmol/L hexakis(2,2-difluoroethoxy)phosphazene was delivered as the sheath liquid at 10 μl/min. ESI-TOFMS was performed in the positive ion mode, and the capillary voltage was set at 4 kV. The flow rate of heated dry nitrogen gas (heater temperature, 300 °C) was maintained at 10 psig. For TOFMS, the fragmenter, skimmer and Oct RFV voltages were set at 75, 50 and 125 V, respectively. Automatic recalibration of each acquired spectrum was achieved using the masses of reference standards ([^{13}C isotopic ion of a protonated methanol dimer (2MeOH + H)]$^+$, *m/z* 66.0632 and [hexakis(2,2-difluoroethoxy) phosphazene + H]$^+$, *m/z* 622.0290). Exact mass data were acquired at a rate of 1.5 spectra/s over a 50–1000 *m/z* range. To facilitate peak identification and quantification, we analyzed 162 commercially available metabolic standards before analyzing the samples. The raw data were processed using our proprietary software (MasterHands) [17].

2.3. *Liquid chromatography tandem mass spectrometry (LC–MS/MS) technique for analysis of serum γ-glutamyl peptide*

LC–MS/MS was carried out using an Agilent 1100 series HPLC system (Agilent Technologies) and an API 3000 triple-quadrupole tandem mass spectrometer (Applied Biosystems, Foster City, CA). System control and data acquisition and analyses were performed with the Applied Biosystems Analyst QS software.

The targeted γ-glutamyl peptides were separated on a Develosil RPAQUEOUS-AR-3 column (2 mm i.d. × 100 mm, 3 μm; Nomura Chemical, Seto, Japan) that was maintained at 30 °C. The mobile phase consisted of 0.5% formic acid/water as solution A and acetonitrile as solution B. The gradient was increased from 0% B at 0 min to 1% at 5 min, 10% at 15 min and 99% at 17 min and then retained at 99% until 19 min. The flow rate was 0.2 ml/min and the injection volume was 1 μl. The MS conditions for positive ions were: mode, multiple reaction monitoring (MRM); ion spray voltage, 5.5 kV; nebulizer gas, 12 psi; curtain gas, 8 psi; collision gas, 8 U; nitrogen gas temperature, 550 °C. The MRM parameters, i.e. Q1 (protonated precursor ion), Q3 (production), declustering potential, focusing potential, collision energy and collision cell exit potential for γ-glutamyl peptides, were optimized using the Analyst software.

2.4. *Principal component analysis and heat map visualization*

Principal component analysis, which is a type of unsupervised statistical analysis used widely as a statistical tool in metabolomics studies, was applied prior to the detailed data analysis [18]. This facilitates visual inspection of the distributed samples in principal component (PC) space using score plots [19], and the distance between individual samples in score plots reflects the degree of systematic variation in metabolite profiles among samples. Principal component analysis converts high-dimensional data into fewer dimensions, by projecting the data into a reduced dimensional subspace, while maintaining as much variance from the original data as possible [20]. In this study, the procedure was repeated until the datasets were presented within three dimensions. We also visualized the observed metabolomic profile as a heat map representation, and performed hierarchical clustering analysis. The metabolite concentrations were averaged in each group, and the colors on the heat map were determined by subtracting the mean over four groups after log2 transformation. Euclidean distance was used for clustering metabolites.

Table 1 – Patient characteristics according to the virological response.

	Virological response		
	non-virological responder	sustained virological responder	*p* value
Number of patient	10	10	
Sex (Male/Female)	2/8	4/6	NS[a]
Age	55.3 ± 9.0	50.2 ± 9.9	NS[b]
Height	158.5 ± 9.1	160.5 ± 9.8	NS[b]
Weight	52.0 ± 11.8	58.7 ± 11.3	NS[b]
HCV genotype 1b	10	10	
HCV-RNA > 5 logIU/ml	10	10	
AST	51.9 ± 18.7	51.8 ± 27.5	NS[b]
ALT	64.3 ± 34.2	79.0 ± 52.9	NS[b]
GGT	66.3 ± 42.7	43.1 ± 36.6	NS[b]
Il28B SNP (Ma/Mi)	4/6	10/0	0.011[a]

IL28B SNP: Ma, major homozygote (T/T), Mi, heterozygote or minor homozygote (T/G or G/G).
Data were expressed as mean ± standard deviation. NS, not significant.
[a] Fisher exact test.
[b] Mann–Whitney *U*-test.

2.5. *Statistical analyses*

The Mann–Whitney *U*-test, Wilcoxon matched-pairs signed rank test, and Fisher exact test were used to assess the statistical significance of differences at a significance level of $p < 0.05$. Receiver operating characteristic (ROC) curve analysis was used for assessing the discrimination ability of individual metabolites. To assess the ability to discriminate SVR from NVR using multiple metabolites determined before treatment, we developed a multiple logistic regression (MLR) model. Metabolites for the MLR model were selected by the forward and backward feature selection method using a threshold of $p < 0.2$ for adding and one of $p > 0.2$ for elimination of metabolites. Bootstrap analysis was conducted to obtain unbiased estimates of the developed model. We used the bootstrapping technique to obtain relatively unbiased estimates; 200 repetitions were generated by random selection of individuals allowing redundancy. We used JMP version 9.0.2 (SAS Institute, Cary, NC) for principal component analysis and development of MLR, Weka version 3.6.4 (The University of Waikato, Hamilton, New Zealand) for bootstrap analysis, Mev TM4 software version 4.8.1 (Dana-Farber Cancer Institute, Boston, MA) for

heatmap visualization, and GraphPad Prism version 6.0.1 (Intuitive Software for Science, San Diego, CA) for ROC curve analysis and box-plot visualization.

3. Results

3.1. *Patient characteristics and virological responses*

The characteristics of patients who showed NVR and SVR are shown in Table 1. All of the patients had HCV genotype 1b infection with a high viral load exceeding 5 logIU/ml. Ten patients showed NVR and 10 achieved SVR. There were no significant differences in sex, age, height, weight, aspartate aminotransferase, ALT or GGT between the two patient groups. The only factor that differed significantly between the NVR and SVR patients was the prevalence of single nucleotide polymorphism of IL28B ($p = 0.011$); in the NVR group, a higher proportion of patients (6/10, 60%) carried the IL28B heterozygote or homozygote with minor alleles of rs8099917 than in the SVR group (0/10, 0%).

3.2. *Principal component analysis of patients before and after pegIFN/RBV therapy*

Principal component analysis demonstrated no significant differences in the pretreatment metabolomics profiles among patients with chronic hepatitis C examined before the start of PegIFN/RBV therapy, even between those who subsequently showed NVR and SVR (Fig. 1). When principal component (PC) analysis was applied to compare the changes in the metabolomics profiles before pegIFN/RBV therapy with those after the therapy, significant differences were evident, the first PC being significantly decreased and the third PC significantly increased in both the NVR and SVR patients (Fig. 2). The change in the distribution area of samples reflected these results, becoming narrower after treatment than before treatment, particularly in SVR cases (Fig. 3). This indicated a

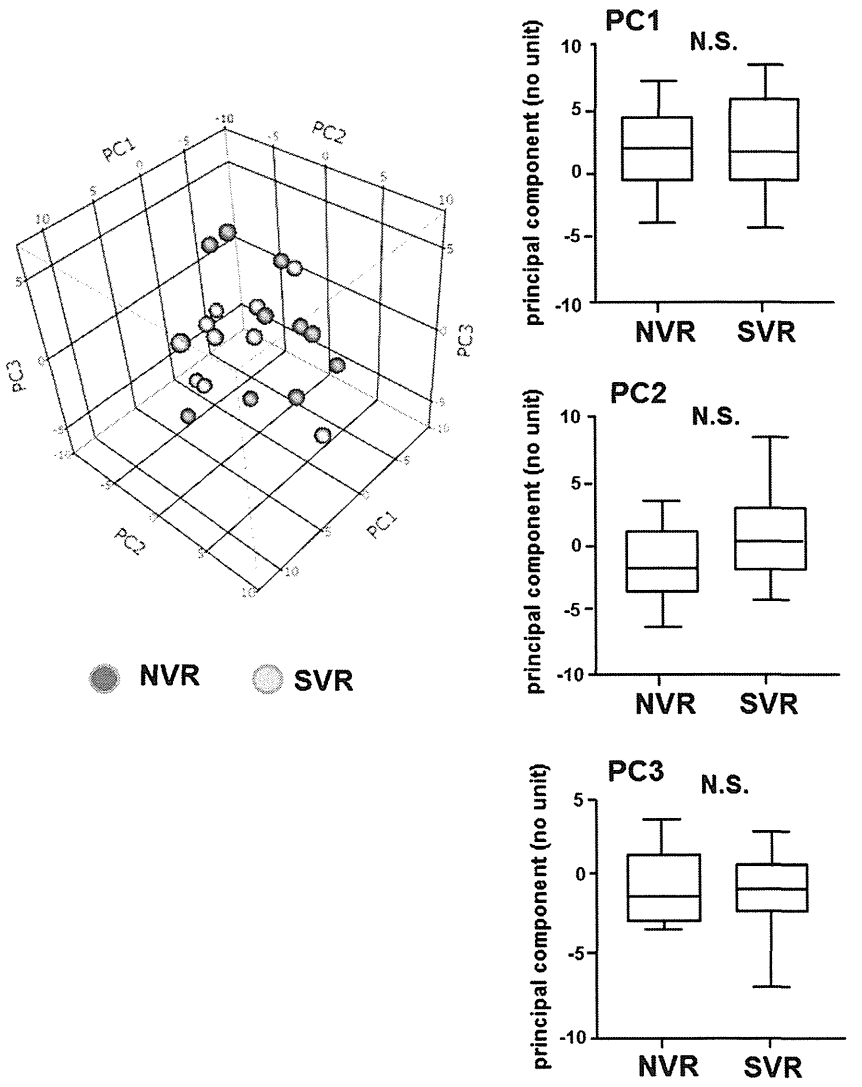

Fig. 1 – Principal component analysis of serum metabolites in the enrolled patients. No significant differences in the pretreatment metabolomics profiles were found between patients who subsequently showed a non-virological response (NVR) and those who achieved a sustained virological response (SVR). Mann–Whitney U-test.

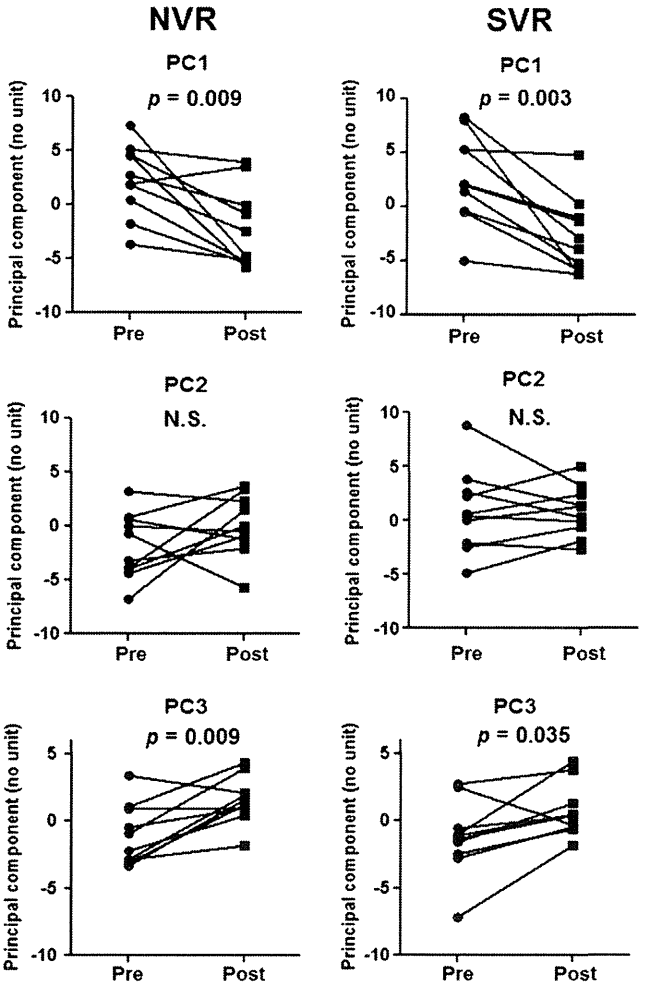

Fig. 2 – Changes in metabolomics profiles 24 weeks after pegIFN/RBV therapy compared with those before therapy. Pre and post indicate pretreatment and post-treatment, respectively. Principal component (PC) 1 was significantly decreased and PC 3 was significantly increased in both the NVR and SVR patients. Wilcoxon matched-pairs signed rank test.

loss of variation in cell metabolism among sustained virological responders, reflecting the fact that cell function had reached a state close to equilibrium as a result of successful HCV eradication.

3.3. *Comparison of metabolite levels in pretreatment serum between non-virological responders and sustained virological responders*

The pretreatment serum level of each metabolite in patients who received PegIFN/RBV therapy was compared between the NVR and SVR groups. We conducted ROC curve analysis to calculate the area under the ROC curve (AUC) values for all metabolites, and only four metabolites – tryptophan, glycine, γ-butyrobetaine and guanidoacetate – showed significant ($p < 0.05$) discrimination abilities (Supplementary Figure 1). Serum concentrations of all four of these metabolites were significantly higher in sustained virological responders than in non-virological responders ($p < 0.05$) (trypytophan: 39.7 ± 4.3 vs. 46.4 ± 6.4, p = 0.010; glycine: 168.7 ± 34.8 vs. 232.6 ± 77.0, p = 0.018; γ-butyrobetaine: 1.5 ± 0.2 vs. 1.8 ± 0.4, p = 0.049; guanidoacetate: 1.7 ± 0.5 vs. 2.1 ± 0.6, p = 0.049, NVR vs. SVR, mean ± standard deviation) (Fig. 4). The AUC values of the four metabolites for discriminating SVR from NVR were 0.84 (95% confidential interval (CI), 0.66–1.02, p = 0.010) for tryptophan, 0.78 (95% CI, 0.57–0.99, p = 0.034) for glycine, 0.76 (95% CI, 0.53–0.99, p = 0.049) for γ-butyrobetaine and 0.76 (95% CI, 0.55–0.98, p = 0.049) for guanidoacetate, all being significant (Fig. 5). We also evaluated the discrimination ability of combinations of multiple serum metabolites using MLR analysis. Among all metabolites, tryptophan and γ-glutamate-arginine were selected for the MLR model by stepwise feature selection methods. The ROC curve for the MLR model incorporating the pretreatment levels of these two metabolites for discriminating SVR from NVR showed a high and significant AUC value (AUC = 0.92, 95% CI, 0.79–1.05, p = 0.002) (Fig. 6). The mean AUC values obtained by bootstrap analysis remained high (AUC = 0.94, 95% CI, 0.93–0.95), indicating that the MLR model showed better accuracy for discriminating SVR from NVR in patients receiving PegIFN/RBV therapy for chronic hepatitis C.

3.4. *Comparison of serum levels of tryptophan between non-virological responders and sustained virological responders carrying an IL28B homozygote for major alleles of rs8099917*

The IL28B genotype is a strong host factor influencing the virological response of HCV to PegIFN/RBV therapy [21,22]. Patients carrying an IL28B homozygote for the major alleles of rs8099917 show a greater propensity to achieve SVR than those carrying an IL28B heterozygote or homozygote for its minor allele. To investigate whether the pretreatment serum level of tryptophan, which was the factor found to differ most significantly between NVR and SVR patients by analyses, was influenced by IL28B genotype, the pretreatment levels of tryptophan in patients with the IL28B homozygote for the major alleles of rs8099917 were compared between four of the 10 non-virological responders and all of the 10 sustained virological responders. The serum levels of tryptophan were significantly higher in the sustained virological responders harboring the major homozygote than in non-virological responders harboring the major homozygote (NVR vs. SVR, 37.8 ± 5.0 vs. 46.4 ± 6.4, p = 0.023) (Fig. 7). Thus the pretreatment level of tryptophan was not influenced by the IL28B genotype.

3.5. *Changes in levels of metabolites influencing the viral response after PegIFN/RBV therapy*

Changes in the serum levels of four metabolites – tryptophan, glycine, γ-butyrobetaine and guanidoacetate – whose pretreatment levels had been shown to differ significantly between the NVR and SVR groups, were examined at 24 weeks after completion of PegIFN/RBV therapy. The serum levels of all four metabolites after PegIFN/RBV therapy did not differ significantly from those before therapy in either NVR or SVR patients. Notably, there was little difference in the

serum level of tryptophan before and after the treatment (SVR: 46.4 ± 6.4 vs. 48.3 ± 12.0, p = 0.88, NVR: 39.7 ± 4.3 vs. 39.9 ± 8.1, p = 0.71, pretreatment vs. post-treatment). This suggests that the pretreatment levels of these metabolites, particularly tryptophan, may help to predict the therapeutic effect of this therapy.

3.6. *Dynamics of serum metabolite levels in patients with chronic hepatitis C before and after PegIFN/RBV therapy*

The dynamics of serum metabolite profile in patients with chronic hepatitis C before and after PegIFN/RBV therapy are shown as a heatmap in Fig. 8. Specific metabolites that showed changes in their serum levels as a result of PegIFN/RBV therapy were determined. The serum levels of four γ-glutamyl dipeptides (γ-Glu-His, γ-Glu-Lys, γ-Glu-Phe, γ-Glu-Val), glutamic acid, 5-oxoproline, glucosamine and methionine sulfoxide were decreased significantly ($p < 0.05$) at 24 weeks after completion of PegIFN/RBV therapy in both non-virological responders and sustained virological responders (Supplementary Figure 2). The serum levels of GGT were decreased significantly at 24 weeks after completion of PegIFN/RBV therapy in sustained virological responders (pretreatment vs. post-treatment: 43.1 ± 31.6 vs. 23.4 ± 8.0, p = 0.028). On the other hand, those of 5-methoxy-3-indoleacetate, glutamine, kynurenine and lysine were increased significantly ($p < 0.05$) in both groups at the same time point (Supplementary Figure 3).

4. Discussion

In this study, we demonstrated that PegIFN/RBV therapy for chronic hepatitis C altered the metabolism of cells in the liver of treated patients. These changes were confirmed by both principal component analysis of the overall metabolome and the dynamics of specific metabolites in serum associated with oxidative stress.

Principal component analysis of metabolites has been shown to be a powerful bioinformatics tool for providing an overall picture of cell metabolic status in individual patients [18–20]. Three-dimensional principle component analysis of metabolites demonstrated no differences in such profiling among the patients enrolled in this study. Twenty four weeks after completion of PegIFN/RBV therapy, principal component analysis demonstrated convergence of these metabolites in the score plots, suggesting that cell function became more homogeneous after completion of the therapy in comparison with the situation before therapy. In particular, the score plot area of the metabolites became narrower in patients who achieved successful HCV eradication. These data suggest that PegIFN/RBV therapy is able to modify the cell function of such patients, so that it approximates the normal function seen in healthy individuals.

The effect of PegIFN/RBV therapy on the viremia in patients with chronic hepatitis C is affected by various host factors. Therefore we considered that it would be informative to

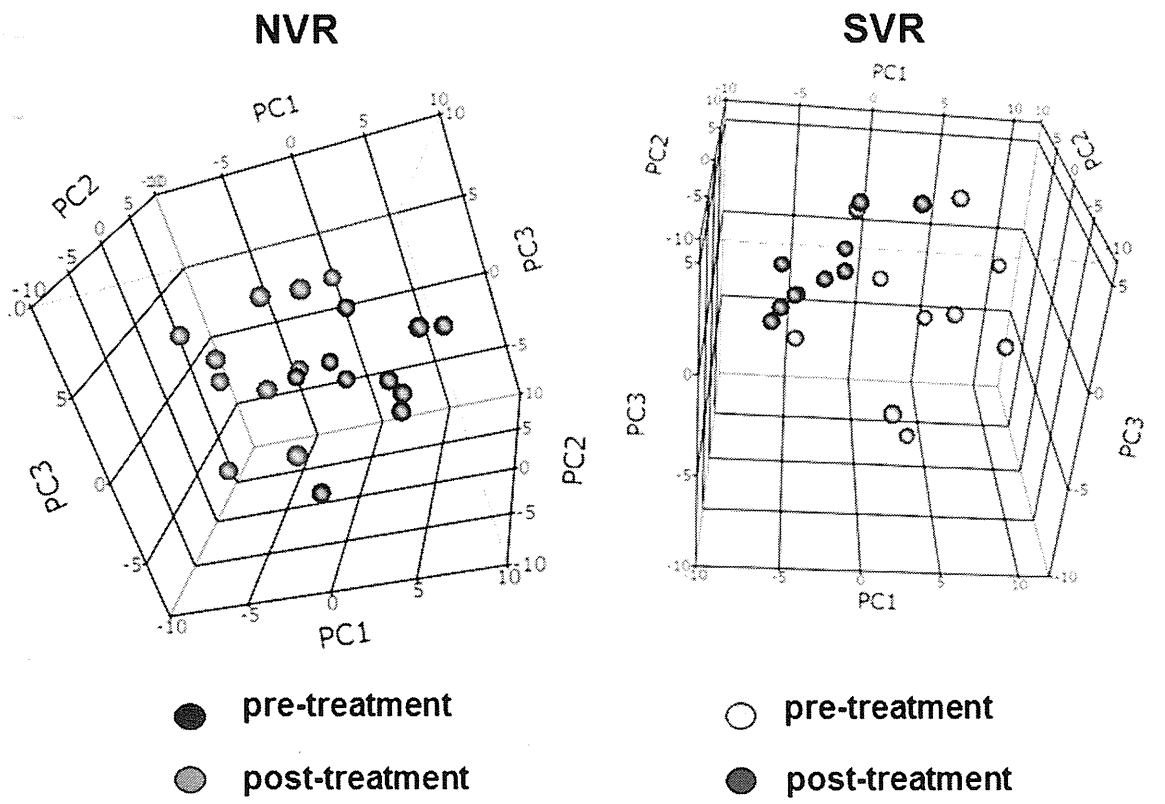

Fig. 3 – Principal component analysis of changes in serum metabolites 24 weeks after pegIFN/RBV therapy (post-treatment) compared with those before therapy (pretreatment). The distribution area of samples became narrower after therapy relative to that before therapy, and this change was particularly obvious in SVR cases.

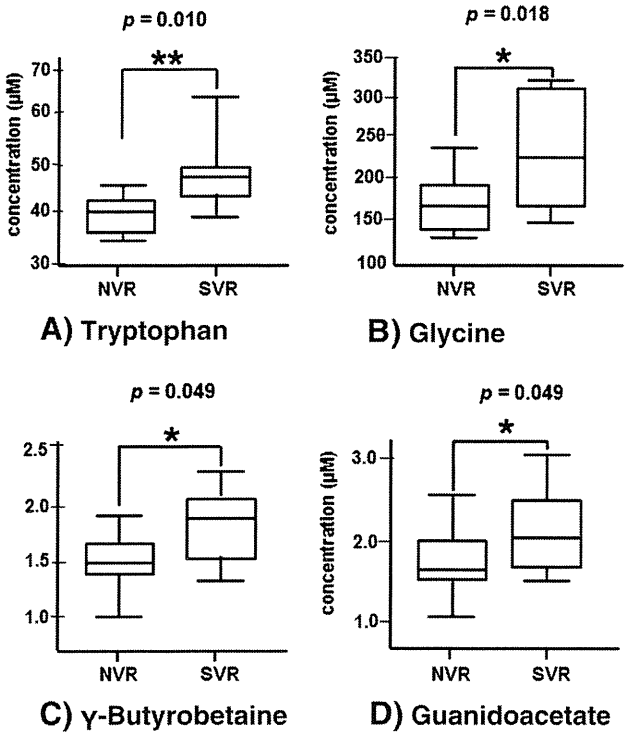

Fig. 4 – Comparison of metabolite levels in serum before treatment between the NVR and SVR patients. The serum levels of tryptophan, glycine, γ-butyrobetaine and guanidoacetate were significantly higher in SVR patients than in NVR patients ($p < 0.05$). Mann–Whitney *U*-test.

investigate whether the cell metabolic status of patients before the start of treatment would affect the viral response to PegIFN/RBV therapy. The serum levels of several specific metabolites, including tryptophan, glycine, γ-butyrobetaine and guanidoacetate, were significantly higher in the sustained virological responders than in non-virological responders,

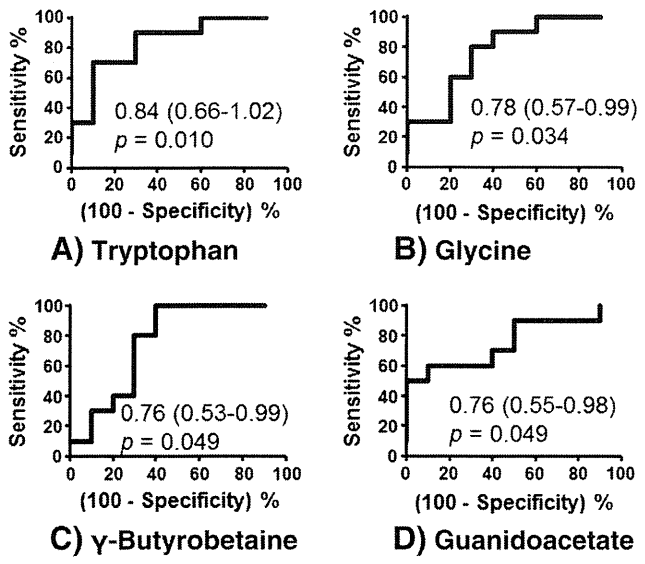

Fig. 5 – ROC curve analyses of four metabolites that were able to discriminate SVR from NVR.

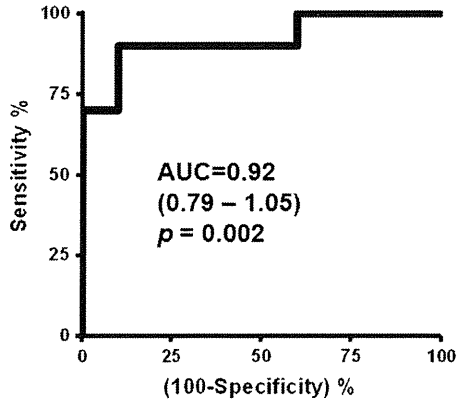

Fig. 6 – ROC curve of multiple logistic regression model incorporating the pretreatment levels of tryptophan and γ-glutamate-arginine for discriminating SVR from NVR.

although principal component analysis revealed no significant difference in the total metabolite profile between them. Our MLR analysis selected two metabolites – tryptophan and γ-glutamate-arginine – that were able to predict the viral response with some degree of accuracy. Although a further study with a larger cohort will be needed in order to confirm whether the serum levels of these metabolites are indeed associated with antiviral effect of PegIFN/RBV therapy, some of them, particularly tryptophan, have already been suggested to have such a relationship.

Tryptophan is a source of kynurenine derivatives, and the pathway responsible is dependent on indoleamine 2,3-dioxygenase (IDO) [23,24]. IDO is inducible in a large variety of cells by inflammatory cytokines such as IFN-γ, and therefore tryptophan degradation is accelerated by infection or malignant diseases that are accompanied by cellular immune activation [25,26]. IDO plays an important role in suppression of the cellular immune response [27,28], and can inhibit T-cell responses, thereby inducing immunological tolerance [29]. Genetic variants affecting serum metabolite levels may play a functional role in the liver [30]. Although no previous study

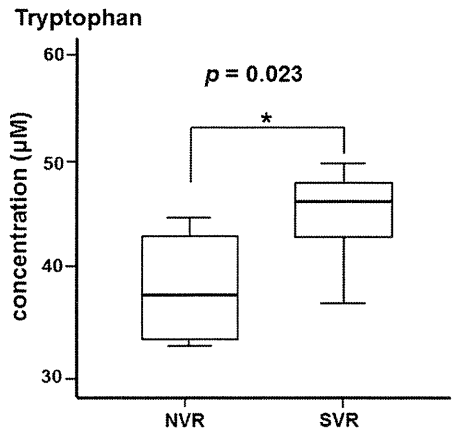

Fig. 7 – Comparison of the serum levels of tryptophan between NVR and SVR patients carrying IL28B homozygotes for the major alleles of rs8099917. Mann–Whitney *U*-test.

has investigated genetic differences associated with the degree of IDO induction, non-virological responders with low tryptophan levels due to active tryptophan degradation may be in a state of down-regulation of the immune response in the presence of an increased amount of inducible IDO, which in turn may be partly associated with low responsiveness to IFN-based antiviral therapy. The difference in the serum levels of tryptophan between the NVR and SVR groups in the present study was not related to IL28B genotype. These data suggest that the metabolic status of liver cells represented by differences in the serum metabolite profiles between NVR and SVR may predict the therapeutic effect of PegIFN/RBV on chronic hepatitis C.

This study identified for the first time the specific metabolites in serum whose levels were altered in patients with chronic hepatitis C receiving PegIFN/RBV therapy. We found that PegIFN/RBV therapy reduced the serum levels of four γ-glutamyl dipeptides (γ-Glu-His, γ-Glu-Lys, γ-Glu-Phe, γ-Glu-Val), glutamic acid, 5-oxoproline, glucosamine, and methionine sulfoxide. The γ-glutamyl dipeptides are formed by binding of glutamic acid to various amino acids catalyzed by γ-glutamylcysteine synthetase, and are produced as a by-product of glutathione, which has a protective effect against oxidative stress [15,31,32]. The γ-glutamyl cycle is activated by glutathione production in patients with liver diseases such as hepatitis, the glutathione being consumed to neutralize generated ROS, in turn leading to activation of γ-glutamylcysteine synthetase, and resulting in the biosynthesis of glutathione together with γ-glutamyl dipeptides [15]. This would suggest that PegIFN/RBV therapy removes oxidative stress and alters cell metabolism towards a more normal range as a result of reduced glutathione production, as was shown by principal component analysis in the present study. In addition, the serum level of GGT has been widely used as a marker of liver dysfunction, alcohol intake, or metabolic syndrome, and it can be also used as an indicator of amelioration of oxidative stress [16]. To investigate the γ-glutamyl dipeptide biosynthetic pathway, we previously performed trace analyses of γ-Glu-X and γ-Glu-X-Gly peptides by intraperitoneal injection of labeled threonine and acetaminophen [15]. The rapid decrease of labeled threonine and the gradual increasing of the labeled γ-Glu-X-Gly/γ-Glu-X ratio indicated that γ-glutamyl peptides were synthesized in the order γ-Glu-X > γ-Glu-X-Gly [15], suggesting that γ-Glu-X was synthesized rather than being a product of γ-Glu-X-Gly catalysis by GGT. Previous studies have reported that an improvement of the serum GGT level leads to a decrease of free radical production, and that the baseline level of GGT is associated with the response to IFN-based antiviral therapy in chronic hepatitis C [33–35]. In the present study, the pretreatment serum levels of GGT in non-virological responders had a tendency to be higher than those of sustained virological responders, and they were significantly decreased after successful treatment. These results suggest that this therapy helps remove oxidative stress.

On the other hand, the serum levels of 5-methoxy-3-indoleacetate, glutamine, kynurenine and lysine were increased significantly 24 weeks after completion of PegIFN/RBV therapy in both non-virological responders and sustained virological responders. These changes may have resulted from the improvement of cell metabolism by the therapy. The removal of the oxidative stress reflected production of glutamine and lysine. Improvement of tryptophan metabolism through the anti-inflammatory effect of PegIFN/RBV therapy is thought to normalize the production of kynurenine from tryptophan [23–26]. Also, the improvement of liver steatosis as a result of reduced expression of HCV core protein may generate an increase of 5-methoxy-3-indoleacetate, which binds to, and activates, peroxisome proliferator-activated receptor-γ [36,37]. Oxidative stress plays an important role in the progression of liver inflammation and hepatocarcinogenesis [8,38], including that associated with HCV infection [10–12]. The results of the present study suggest that PegIFN/RBV therapy can slow the progression of liver disease in patients with chronic HCV infection through reduction of oxidative stress.

In conclusion, the present study has shown that the pretreatment serum levels of low-molecular-weight metabolites, including tryptophan, are associated with the virological response to PegIFN/RBV therapy, and that such therapy can reduce the level of oxidative stress in patients with chronic HCV infection, as well as modifying the state of cell metabolism. However, further studies are needed to validate the present findings in a larger cohort of patients.

Author contributions

Study design, data analysis and interpretation, writing manuscript: T Saito and Sugimoto equally contributed to this work as the lead author of this manuscript; Study conduct: Soga; Study design and interpretation: M Tomita, Ueno; analysis and interpretation: Igarashi, K Saito, Shao; data collection: Katsumi, K Tomita, Sato, Okumoto, Nishise, Watanabe.

Funding

This work was supported by research grants from the Ministry of Health, Labor and Welfare of Japan, research grants from the Japan Science and Technology Agency, and research funds from the Yamagata Prefectural Government and City of Tsuruoka.

Acknowledgments

We thank Prof. Dr. Sumio Kawata (Hyogo Prefectural Nishinomiya Hospital) for his excellent advice, and Ms. Yayoi Kohno for technical assistance.

Fig. 8 – Heat map of observed metabolomic profiles. Pre and post indicate pretreatment and post-treatment, respectively. Red color indicates metabolite concentrations that were higher than average, while blue color indicates those that were lower than average. The order of the metabolites was arranged on the basis of clustering analysis.

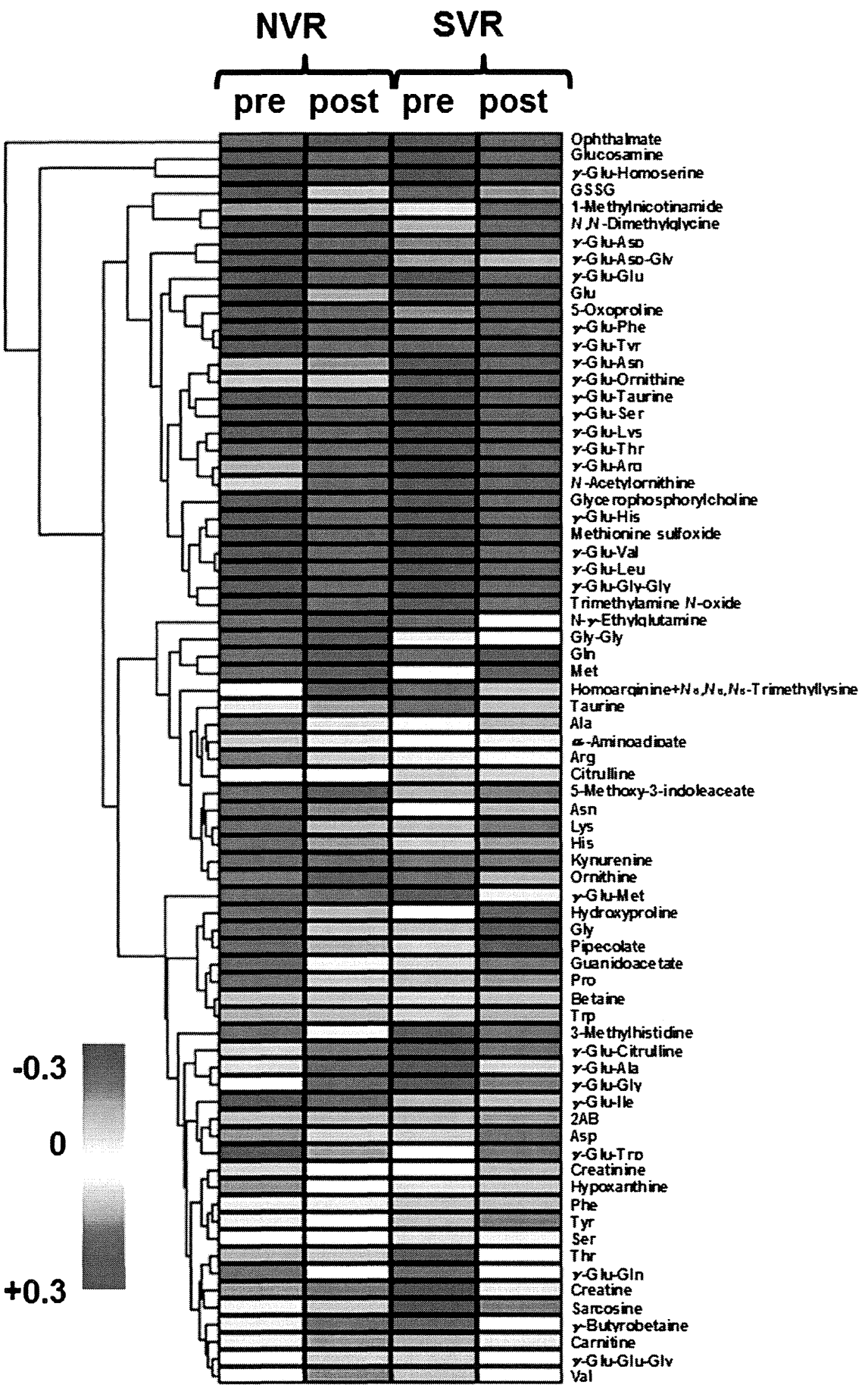
NVR
SVR
pre
post
pre
post
Ophthalmate
Glucosamine
γ-Glu-Homoserine
GSSG
1-Methylnicotinamide
N,N-Dimethylglycine
γ-Glu-Asp
γ-Glu-Asp-Gly
γ-Glu-Glu
Glu
5-Oxoproline
γ-Glu-Phe
γ-Glu-Tyr
γ-Glu-Asn
γ-Glu-Ornithine
γ-Glu-Taurine
γ-Glu-Ser
γ-Glu-Lys
γ-Glu-Thr
γ-Glu-Arg
N-Acetylornithine
Glycerophosphorylcholine
γ-Glu-His
Methionine sulfoxide
γ-Glu-Val
γ-Glu-Leu
γ-Glu-Gly-Gly
Trimethylamine N-oxide
N-γ-Ethylglutamine
Gly-Gly
Gln
Met
Homoarginine+Nε,Nε,Nε-Trimethyllysine
Taurine
Ala
α-Aminoadipate
Arg
Citrulline
5-Methoxy-3-indoleacetate
Asn
Lys
His
Kynurenine
Ornithine
γ-Glu-Met
Hydroxyproline
Gly
Pipecolate
Guanidoacetate
Pro
Betaine
Trp
3-Methylhistidine
γ-Glu-Citrulline
γ-Glu-Ala
γ-Glu-Gly
γ-Glu-Ile
2AB
Asp
γ-Glu-Trp
Creatinine
Hypoxanthine
Phe
Tyr
Ser
Thr
γ-Glu-Gln
Creatine
Sarcosine
γ-Butyrobetaine
Carnitine
γ-Glu-Glu-Gly
Val
-0.3
0
+0.3

Conflict of interest

The authors have no conflict of interest.

Appendix A. Supplementary data

Supplementary data to this article can be found online at http://dx.doi.org/10.1016/j.metabol.2013.07.002.

REFERENCES

[1] Di Bisceglie AM, Goodman ZD, Ishak KG, et al. Long-term clinical and histopathological follow-up of chronic post-transfusion hepatitis. Hepatology 1991;14:969–74.

[2] Kiyosawa K, Sodeyama T, Tanaka E, et al. Interrelationship of blood transfusion, non-A, non-B hepatitis and hepatocellular carcinoma: analysis by detection of antibody to hepatitis C virus. Hepatology 1990;12:671–5.

[3] Imai Y, Kawata S, Tamura S, et al. Relation of interferon therapy and hepatocellular carcinoma in patients with chronic hepatitis C. Osaka Hepatocellular Carcinoma Prevention Study Group. Ann Intern Med 1998;129:94–9.

[4] Omata M, Yoshida H, Shiratori Y. Prevention of hepatocellular carcinoma and its recurrence in chronic hepatitis C patients by interferon therapy. Clin Gastroenterol Hepatol 2005;3(10 Suppl 2):S141–3.

[5] Lok AS, Everhart JE, Wright EC, et al. Maintenance peginterferon therapy and other factors associated with hepatocellular carcinoma in patients with advanced hepatitis C. Gastroenterology 2011;140:840–9.

[6] Watanabe S, Enomoto N, Koike K, et al. Cancer preventive effect of pegylated interferon α-2b plus ribavirin in a real-life clinical setting in Japan: PERFECT interim analysis. Hepatol Res 2011;41:955–64.

[7] Qu LS, Chen H, Kuai XL, et al. Effects of interferon therapy on development of hepatocellular carcinoma in patients with hepatitis C-related cirrhosis. A meta-analysis of randomized controlled trials. Hepatol Res 2012;42:782–9.

[8] Jaeschke H. Reactive oxygen and mechanisms of inflammatory liver injury: present concepts. J Gastroenterol Hepatol 2011;26(Suppl 1):173–9.

[9] Choi J. Oxidative stress, endogenous antioxidants, alcohol, and hepatitis C: pathogenic interactions and therapeutic considerations. Free Radic Biol Med 2012;52:1135–50.

[10] Fujinaga H, Tsutsumi T, Yotsuyanagi H, et al. Hepatocarcinogenesis in hepatitis C: HCV shrewdly exacerbates oxidative stress by modulating both production and scavenging of reactive oxygen species. Oncology 2011;81(Suppl 1):11–7.

[11] Romilda C, Marika P, Alessandro S, et al. Oxidative DNA damage correlates with cell immortalization and mir-92 expression in hepatocellular carcinoma. BMC Cancer 2012;12:177.

[12] Tsukiyama-Kohara K. Role of oxidative stress in hepatocarcinogenesis induced by hepatitis C virus. Int J Mol Sci 2012;13:15271–8.

[13] Soga T, Baran R, Suematsu M, et al. Differential metabolomics reveals ophthalmic acid as an oxidative stress biomarker indicating hepatic glutathione consumption. J Biol Chem 2006;281:16768–76.

[14] Shintani T, Iwabuchi T, Soga T, et al. Cystathionine beta-synthase as a carbon monoxide-sensitive regulator of bile excretion. Hepatology 2009;49:141–50.

[15] Soga T, Sugimoto M, Honma M, et al. Serum metabolomics reveals γ-glutamyl dipeptides as biomarkers for discrimination among different forms of liver disease. J Hepatol 2011;55:896–905.

[16] Whitfield JB. Gamma glutamyl transferase. Crit Rev Clin Lab Sci 2001;38:263–355.

[17] Sugimoto M, Wong DT, Hirayama A, et al. Capillary electrophoresis mass spectrometry-based saliva metabolomics identified oral, breast and pancreatic cancer-specific profiles. Metabolomics 2010;6:78–95.

[18] Sugimoto M, Kawakami M, Robert M, et al. Bioinformatics tools for mass spectroscopy-based metabolomic data processing and analysis. Curr Bioinform 2012;7:96–108.

[19] Blekherman G, Laubenbacher R, Cortes DF, et al. Bioinformatics tools for cancer metabolomics. Metabolomics 2011;7:329–43.

[20] Nyamundanda G, Brennan L, Gormley IC. Probabilistic principal component analysis for metabolomic data. BMC Bioinformatics 2010;11:571.

[21] Ge D, Fellay J, Thompson AJ, et al. Genetic variation in IL28B predicts hepatitis C treatment-induced viral clearance. Nature 2009;461:399–401.

[22] Tanaka Y, Nishida N, Sugiyama M, et al. Genome-wide association of IL28B with response to pegylated interferon-alpha and ribavirin therapy for chronic hepatitis C. Nat Genet 2009;41:1105–9.

[23] Tankiewicz A, Pawlak D, Buczko W. Enzymes of the kynurenine pathway. Postepy Hig Med Dosw 2001;55:715–31.

[24] Thackray SJ, Mowat CG, Chapman SK. Exploring the mechanism of tryptophan 2,3-dioxygenase. Biochem Soc Trans 2008;36:1120–3.

[25] Taylor MW, Feng GS. Relationship between interferon-gamma, indoleamine 2,3-dioxygenase, and tryptophan catabolism. FASEB J 1991;5:2516–22.

[26] Wirleitner B, Neurauter G, Schrocksnadel K, et al. Interferon-γ-induced conversion of tryptophan: immunologic and neuropsychiatric aspects. Curr Med Chem 2003;10:1581–91.

[27] Mándi Y, Vécsei L. The kynurenine system and immunoregulation. J Neural Transm 2012;119:197–209.

[28] Liu H, Liu L, Liu K, et al. Reduced cytotoxic function of effector CD8+ T cells is responsible for indoleamine 2,3-dioxygenase-dependent immune suppression. J Immunol 2009;183:1022–31.

[29] Brandacher G, Margreiter R, Fuchs D. Implications of IFN-gamma-mediated tryptophan catabolism on solid organ transplantation. Curr Drug Metab 2007;8:273–82.

[30] Mirkov S, Myers JL, Ramirez J, et al. SNPs affecting serum metabolomic traits may regulate gene transcription and lipid accumulation in the liver. Metabolism 2012;61:1523–7.

[31] Griffith OW, Meister A. Potent and specific inhibition of glutathione synthesis by buthionine sulfoximine (S-n-butyl homocysteine sulfoximine). J Biol Chem 1979;254:7558–60.

[32] Zalups RK, Lash LH. Depletion of glutathione in the kidney and the renal disposition of administered inorganic mercury. Drug Metab Dispos 1997;25:516–23.

[33] Van Thiel DH, Freidlander L, Malloy P, et al. gamma-Glutamyl transpeptidase as a response predictor when using alpha-interferon to treat hepatitis C. Hepatogastroenterology 1995;42:888–92.

[34] Bergmann JF, Vrolijk JM, van der Schaar P, et al. γ-Glutamyltransferase and rapid virological response as predictors of successful treatment with experimental or standard peginterferon-α-2b in chronic hepatitis C non-responders. Liver Int 2007;27:1217–25.

[35] Paolicchi A, Marchi S, Petruccelli S, et al. Gamma-glutamyltransferase in fine-needle liver biopsies of subjects with chronic hepatitis C. J Viral Hepat 2005;12:269–73.

[36] Schupp M, Lazar MA. Endogenous ligands for nuclear receptors: digging deeper. J Biol Chem 2010;285:40409–15.

[37] Harmon GS, Lam MT, Glass CK. PPARs and lipid ligands in inflammation and metabolism. Chem Rev 2011;111:6321–40.

[38] Marra M, Sordelli IM, Lombardi A, et al. Molecular targets and oxidative stress biomarkers in hepatocellular carcinoma: an overview. J Transl Med 2011;9:171.

Hepatology Research

Hepatology Research 2013 doi: 10.1111/hepr.12179

Original Article

Prospective comparison of real-time tissue elastography and serum fibrosis markers for the estimation of liver fibrosis in chronic hepatitis C patients

Nobuharu Tamaki,[1] Masayuki Kurosaki,[1] Shuya Matsuda,[1] Toru Nakata,[1] Masaru Muraoka,[1] Yuichiro Suzuki,[1] Yutaka Yasui,[1] Shoko Suzuki,[1] Takanori Hosokawa,[1] Takashi Nishimura,[1] Ken Ueda,[1] Kaoru Tsuchiya,[1] Hiroyuki Nakanishi,[1] Jun Itakura,[1] Yuka Takahashi,[1] Kotaro Matsunaga,[2,4] Kazuhiro Taki,[2] Yasuhiro Asahina[3] and Namiki Izumi[1]

Divisions of [1]Gastroenterology and Hepatology and [2]Pathology, Musashino Red Cross Hospital, [3]Division of Gastroenterology and Hepatology, Tokyo Medical and Dental University, Tokyo and [4]Division of Gastroenterology and Hepatology, St Marianna University School of Medicine, Kanagawa, Japan

Aim: Real-time tissue elastography (RTE) is a non-invasive method for the measurement of tissue elasticity using ultrasonography. Liver fibrosis (LF) index is a quantitative method for evaluation of liver fibrosis calculated by RTE image features. This study aimed to investigate the significance of LF index for predicting liver fibrosis in chronic hepatitis C patients.

Methods: In this prospective study, 115 patients with chronic hepatitis C who underwent liver biopsy were included, and the diagnostic accuracy of LF index and serum fibrosis markers was evaluated.

Results: RTE imaging was successfully performed on all patients. Median LF index in patients with F0–1, F2, F3 and F4 were 2.61, 3.07, 3.54 and 4.25, respectively, demonstrating a stepwise increase with liver fibrosis progression ($P < 0.001$). LF index (odds ratio [OR] = 5.3, 95% confidence interval [CI] = 2.2–13.0) and platelet count (OR = 0.78, 95% CI = 0.68–0.89) were independently associated with the presence of advanced fibrosis (F3–4). Further, LF index was independently associated with the presence of minimal fibrosis (F0–1) (OR = 0.25, 95% CI = 0.11–0.55). The area under the receiver–operator curve (AUROC) of LF index for predicting advanced fibrosis (0.84) was superior to platelets (0.82), FIB-4 index (0.80) and aspartate aminotransferase/platelet ratio index (APRI) (0.76). AUROC of LF index (0.81) was superior to platelets (0.73), FIB-4 index (0.79) and APRI (0.78) in predicting minimal fibrosis.

Conclusion: LF index calculated by RTE is useful for predicting liver fibrosis, and diagnostic accuracy of LF index is superior to serum fibrosis markers.

Key words: chronic hepatitis C, fibrosis, liver fibrosis index, real-time tissue elastography

INTRODUCTION

AN ADVANCED STAGE of liver fibrosis in chronic hepatitis C (CHC) is associated with hepatocellular carcinoma development and complications such as esophageal variceal bleeding and liver failure.[1,2] Therefore, accurate evaluation of the stage of liver fibrosis is most important in clinical practice. Liver biopsy is considered to be the golden standard for diagnosis of liver fibrosis.[3–5] However, this method may be inaccurate because of sampling errors and interobserver variations.[6,7]

Improvements in a variety of non-invasive methods for evaluating liver fibrosis have recently emerged as alternatives to liver biopsy. Liver fibrosis was reportedly predicted by measurement of liver stiffness using transient elastography[8,9] and acoustic radiation force impulse (ARFI).[10,11] As assessed by blood laboratory tests, the aspartate aminotransferase (AST)/alanine

Correspondence: Dr Namiki Izumi, Department of Gastroenterology and Hepatology, Musashino Red Cross Hospital, 1-26-1 Kyonan-cho, Musashino-shi, Tokyo 180-8610, Japan. Email: nizumi@musashino.jrc.or.jp

Conflict of interest: The authors who have taken part in this study declare that they do not have anything to disclose regarding funding or conflict of interest with respect to this manuscript.

Received 28 January 2013; revision 20 May 2013; accepted 29 May 2013.

aminotransferase (ALT) ratio,[12] AST/platelet ratio index (APRI),[13,14] and FIB-4 index[15,16] have been reported to be useful for the prediction of liver fibrosis. We previously reported that the FIB-4 index is useful for the prediction of liver fibrosis progression.[17]

Real-time tissue elastography (RTE) is a non-invasive method for the measurement of tissue elasticity using ultrasonography.[18] RTE calculates the relative hardness of tissue from the degree of tissue distortion and displays this information as a color image. RTE was recently reported to be useful for predicting liver fibrosis.[19,20] To increase the objectivity of the evaluation, an image analysis method to evaluate the strain image features and a new algorithm to deliver an index were proposed. Liver fibrosis (LF) index is a quantitative method for evaluation of liver fibrosis that is calculated by nine RTE image features, and the significance of LF index for predicting liver fibrosis has been reported.[21,22]

In the present study, we prospectively investigated the significance of LF index calculated by RTE for the prediction of liver fibrosis in CHC patients. Further, diagnostic accuracy for liver fibrosis was compared between LF index and serum fibrosis markers.

METHODS

Patients

A TOTAL OF 127 consecutive patients with CHC were prospectively investigated. All patients underwent liver biopsy at Musashino Red Cross Hospital between February 2011 and November 2012. Exclusion criteria comprised the following: (i) co-infection with hepatitis B virus ($n = 1$); (ii) co-infection with HIV ($n = 1$); (iii) history of autoimmune hepatitis or primary biliary cirrhosis ($n = 3$); (iv) alcohol abuse (intake of alcohol equivalent to pure alcohol ≥40 g/day) ($n = 0$); (v) portal tracts of biopsy sample of less than five ($n = 7$); and (vi) presence of serious heart disease ($n = 0$). After exclusion, 115 patients were enrolled in this study. Written informed consent was obtained from each patient and the study protocol conformed to the ethical guidelines of the Declaration of Helsinki and was approved by the institutional ethics review committees (application no. 24007).

Histological evaluation

Liver biopsy specimens were laparoscopically obtained using 13-G needles ($n = 93$). When laparoscopy was not conducted due to a history of upper abdominal surgery, percutaneous ultrasound-guided liver biopsy was performed using 15-G needles ($n = 22$). Specimens were fixed, paraffin-embedded, and stained with hematoxylin–eosin and Masson-trichrome. A biopsy sample with minimum portal tracts of five was required for diagnosis. All liver biopsy samples were independently evaluated by two senior pathologists who were blinded to the clinical data. Fibrosis staging was categorized according to the METAVIR score:[23] F0, no fibrosis; F1, portal fibrosis without septa; F2, portal fibrosis with few septa; F3, numerous septa without cirrhosis; and F4, cirrhosis. Activity of necroinflammation was graded on a scale of 0–3: A0, no activity; A1, mild activity; A2, moderate activity; and A3, severe activity. Percentage of steatosis was quantified by determining the average proportion of hepatocytes affected by steatosis and graded on a scale of 0–3: grade 0, no steatosis; grade 1, 1–33%; grade 2, 34–66%; and grade 3, 67% and over.

Clinical and biological data

The age and sex of the patients were recorded. Serum samples were collected within 1 day prior to liver biopsy and the following variables were obtained through serum sample analysis: AST, ALT and platelet count. FIB-4 index and APRI were calculated according to the published formula appropriate to each measure.[13,15]

RTE and LF index

Real-time tissue elastography was performed using HI VISION Preirus (Hitachi Aloka Medical, Tokyo, Japan) and the EUP-L52 linear probe (3–7 MHz; Hitachi Aloka Medical) within 3 days of liver biopsy. RTE was performed on the right lobe of the liver through the intercostal space. An RTE image was induced by heartbeats. Five RTE images were collected for each patient and analyzed to calculate nine image features. RTE method and the equation that calculates LF index using nine image features has been previously detailed.[22] Results are expressed as mean LF index of all measurements. Two hepatologists (N. T. and K. Tsuchiya, with 8 and 16 years of experience, respectively) performed RTE. In 32 patients with CHC, LF index was measured independently by two examiners. The correlation coefficient of LF index between two examiners was 0.85 ($P \leq 0.001$).

Statistical analysis

Correlations between LF index and histological fibrosis stage were analyzed using Spearman's rank correlation coefficients. Categorical variables were compared using Fisher's exact test, and continuous variables were compared using Mann–Whitney *U*-test. $P < 0.05$ was considered statistically significant. Logistic regression was

used for multivariate analysis. Receiver–operator curves (ROC) were constructed, and the area under the ROC (AUROC) was calculated. Optimal cut-off values were selected, to maximize sensitivity, specificity and diagnostic accuracy. Sensitivity, specificity, positive predictive value (PPV) and negative predictive value (NPV) were calculated by using cut-offs obtained by ROC. SPSS software ver. 15.0 (SPSS, Chicago, IL, USA) was used for analyses.

RESULTS

Patient characteristics

THE CHARACTERISTICS OF all 115 patients are listed in Table 1. F0–1 was diagnosed in 52 cases (45%), F2 in 31 (27%), F3 in 20 (17%) and F4 in 12 (11%). Mean values of LF index of F0 (2.62) and F1 (2.60) were not significantly different ($P = 0.9$), and only six patients with F0 were included in this study. Therefore, patients with F0 and F1 were integrated for the analysis. RTE imaging was successfully performed in all patients, and LF index was calculated.

Relationship between histological findings and LF index by RTE

The median value of LF index compared with the METAVIR fibrosis stage is shown in Figure 1. Median LF index in patients with F0–1, F2, F3 and F4 were 2.61, 3.07, 3.54 and 4.25, respectively, demonstrating a stepwise increase with liver fibrosis progression ($P < 0.001$). LF index of each fibrosis stage significantly differed from each other (F0–1 vs F2, $P < 0.001$; F0–1 vs F3, $P < 0.001$; F0–1 vs F4, $P < 0.001$; F2 vs F3, $P = 0.009$; F2 vs F4, $P = 0.001$). On the other hand, mean values of LF index in patients with steatosis grade 0, 1 and 2 were 2.99, 3.29 and 2.60, respectively, demonstrating no significant correlation (Fig. 2a). LF index was compared with steatosis grade for each fibrosis stage. LF index was not significantly different between patients with steatosis and without steatosis (Fig. 2b).

Liver fibrosis index was compared with histological activity. A significant correlation existed between histological activity and fibrosis stage. Therefore, the relationship between LF index and histological activity was examined by each fibrosis stage. In patients with F0–1, the mean LF index of A1, A2 and A3 was 2.60, 2.58 and 2.40, respectively, demonstrating no significant correlation. Similarly, in patients with F2, F3 and F4, there was no significant correlation between LF index and histological activity (Fig. 3).

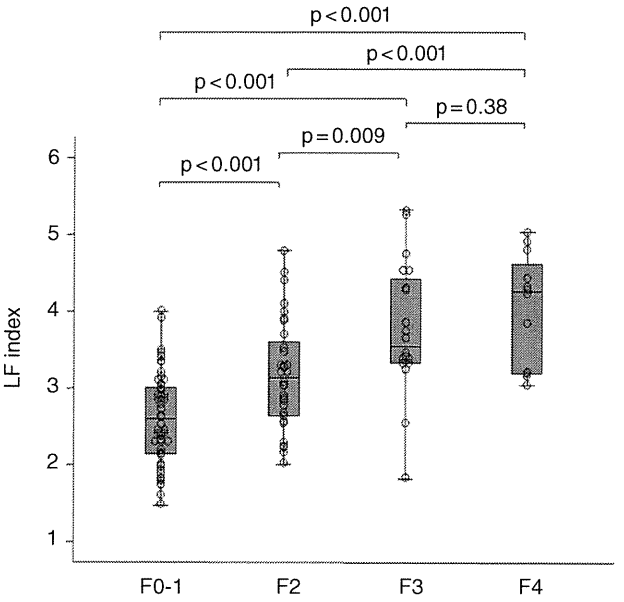

Figure 1 Correlation between liver fibrosis (LF) index calculated by real-time tissue elastography and fibrosis stage. Box plot of the LF index is shown according to each fibrosis stage. The bottom and top of each box represent the 25th and 75th percentiles, giving the interquartile range. The line through the box indicates the median value, and error bar indicates minimum and maximum non-extreme values.

Table 1 Patient characteristics

Characteristics	Patients ($n = 115$)
Female/male	68/47
Age (years)	57.9 ± 10.9
AST (IU/L)	55.7 ± 44.9
ALT (IU/L)	63.2 ± 56.3
Platelet counts ($\times 10^9$/L)	162 ± 53
Portal tracts of biopsy samples	12.6 ± 5.0
Fibrosis stage	
F0–1 (%)	51 (44)
F2 (%)	32 (28)
F3 (%)	20 (17)
F4 (%)	12 (11)
Histological activity	
A0 (%)	0 (0)
A1 (%)	75 (65)
A2 (%)	34 (30)
A3 (%)	6 (5)
Steatosis grade	
Grade 0 (%)	65 (57)
Grade 1 (%)	47 (41)
Grade 2 (%)	3 (2)
Grade 3 (%)	0 (0)

ALT, alanine aminotransferase; AST, aspartate aminotransferase.

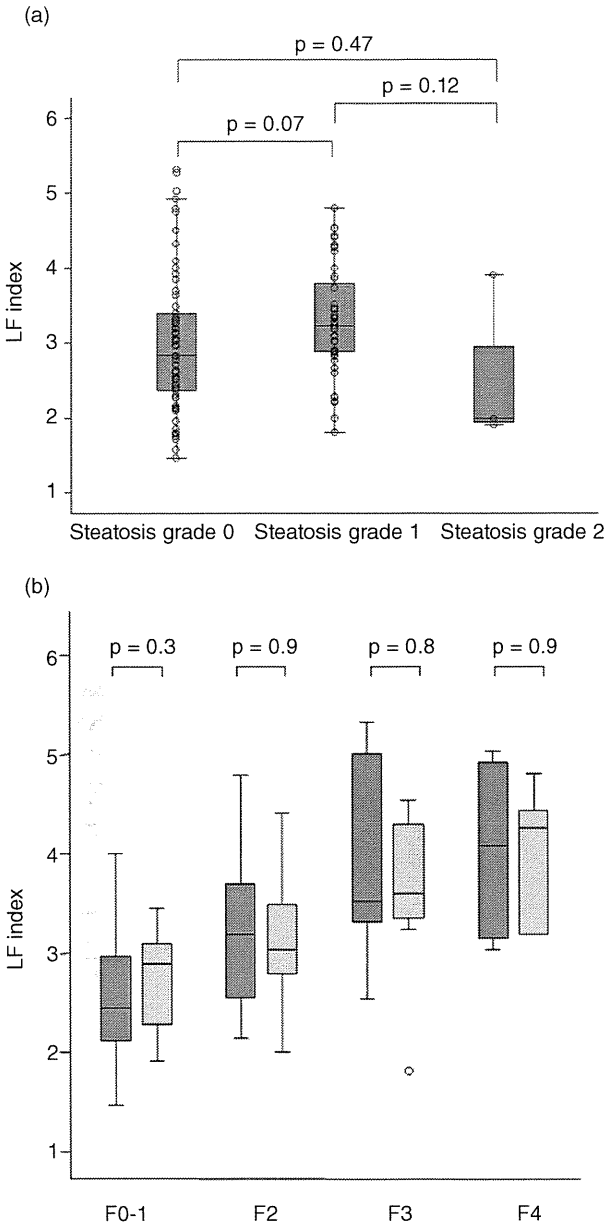

Figure 2 (a) Correlation between liver fibrosis (LF) index and steatosis grade. Box plot of the LF index is shown according to each steatosis grade. The bottom and top of each box represent the 25th and 75th percentiles, giving the interquartile range. The line through the box indicates the median value, and error bar indicates minimum and maximum non-extreme values. (b) Box plot of LF index for each fibrosis stage in relation to degree of steatosis grade. The bottom and top of each box represent the 25th and 75th percentiles, giving the interquartile range. The line through the box indicates the median value, and error bar indicates minimum and maximum non-extreme values. Dark grey bar chart indicates steatosis grade 0. Light grey bar chart indicates steatosis grade 1–2.

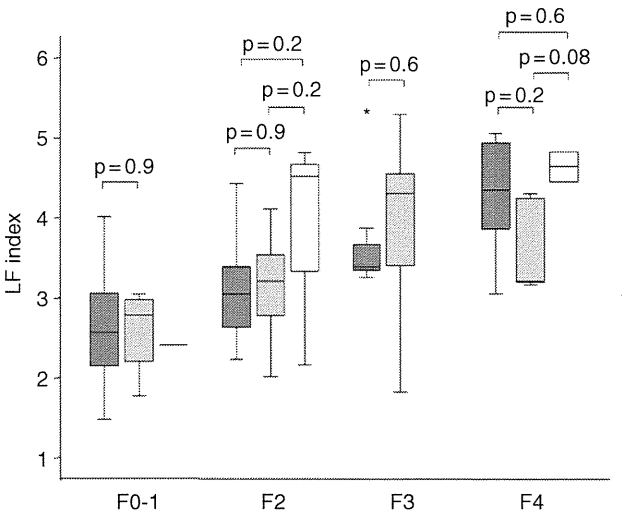

Figure 3 Box plot of liver fibrosis (LF) index for each fibrosis stage in relation to degree of necroinflammatory activity. The bottom and top of each box represent the 25th and 75th percentiles, giving the interquartile range. The line through the box indicates the median value, and error bar indicates minimum and maximum non-extreme values. Dark grey bar chart indicates activity grade 1. Light grey bar chart indicates activity grade 2. White bar chart indicates activity grade 3.

Comparison of variables associated with the presence of advanced fibrosis (F3–4) by univariate and multivariate analysis

Variables associated with the presence of advanced fibrosis (F3–4) were assessed by univariate and multivariate analysis (Table 2). The variables of age ($P = 0.03$) and LF index ($P < 0.001$) were significantly higher, and the variable of platelets ($P < 0.001$) was significantly lower in patients with advanced fibrosis than in patients with F0–2. Multivariate analysis showed that LF index (odds ratio [OR] = 5.3, 95% confidence interval [CI] =2.2–13.0) and platelets (OR = 0.78, 95% CI = 0.68–0.89) were independently associated with the presence of advanced fibrosis.

Comparison of variables associated with the presence of minimal fibrosis (F0–1) by univariate and multivariate analysis

Variables associated with the presence of minimal fibrosis (F0–1) were assessed by univariate and multivariate analysis (Table 3). The variables of age ($P < 0.001$), AST ($P = 0.02$) and LF index ($P < 0.001$) were significantly lower, and the variable of platelets ($P < 0.001$) was significantly higher in F0–1 patients than F2–4 patients.

Table 2 Variables associated with the presence of advanced fibrosis (F3–4) by univariate and multivariate analysis

	F0–2 ($n = 83$)	F3–4 ($n = 32$)	*P*-value (Univariate)	Odds ratio (95% CI) (Multivariate)
Age (years)	56.6 ± 10.9	61.3 ± 10.4	0.03	
Sex (female/male)	51/32	17/15	0.41	
AST (IU/L)	52.3 ± 43.3	64.4 ± 48.3	0.19	
ALT (IU/L)	62.9 ± 60.6	63.9 ± 44.2	0.93	
Platelets ($\times 10^9$/L)	179 ± 47	117 ± 42	<0.001	0.78 (0.68–0.89)
LF index	2.81 ± 0.69	3.86 ± 0.81	<0.001	5.30 (2.16–13.0)

ALT, alanine aminotransferase; AST, aspartate aminotransferase; CI, confidence interval; LF, liver fibrosis.

Multivariate analysis showed that LF index was independently associated with the presence of minimal fibrosis (OR = 0.25, 95% CI = 0.11–0.55).

Diagnostic accuracy of RTE and serum fibrosis markers

Receiver–operator curves of LF index, platelets, FIB-4 index and APRI for predicting advanced fibrosis (F3–4), and minimal fibrosis (F0–1) were plotted, as shown in Figure 4. AUROC of LF index for predicting advanced fibrosis (0.84) was superior to platelets (0.82), FIB-4 index (0.80) and APRI (0.76). Similarly, for predicting minimal fibrosis, AUROC of LF index (0.81) was superior to platelets (0.73), FIB-4 index (0.79) and APRI (0.78). The corresponding sensitivities, specificities, PPV and NPV are detailed in Table 4.

DISCUSSION

IMPROVEMENTS IN VARIOUS methods for prediction of liver fibrosis have recently emerged as alternatives to liver biopsy. RTE is a non-invasive method for the measurement of tissue elasticity using ultrasonography. The utility of RTE for evaluating liver fibrosis is reported in a few studies.[18–22] However, for utilizing LF index, one of the equations used to calculate tissue elasticity by RTE is still unclear. The aim of this study was to investigate the significance of LF index for the prediction of liver fibrosis in CHC patients.

In this prospective study, we found that LF index is a useful predictive factor for diagnosis of the fibrosis stage in CHC patients. Increase in LF index significantly correlated with progression of the fibrosis stage and LF index was able to predict the presence of advanced fibrosis and minimal fibrosis. Previous studies reported the utility of LF index for prediction of the liver fibrosis stage.[21,22] In this study, LF index differed significantly between patients with F0–1 and F2; thus, LF index was especially useful for prediction of minimal fibrosis. This may be due to a sufficient number of patients with F0–1 and F2 included in the present study. This is an advantage of LF index because other quantitative methods by RTE could not discriminate patients with F0–1 and F2.[19,20] On the other hand, there is a possibility that a similar result may be obtained for differentiation of F3 and F4 if a large number of patients with advanced fibrosis was included.

Previous studies did not compare the diagnostic accuracy of LF index and serum fibrosis markers. We revealed that LF index performed better than serum fibrosis

Table 3 Variables associated with the presence of minimal fibrosis (F0–1) by univariate and multivariate analysis

	F0–1 ($n = 51$)	F2–4 ($n = 64$)	*P*-value (Univariate)	Odds ratio (95% CI) (Multivariate)
Age (years)	54.0 ± 11.9	61.0 ± 9.0	<0.001	
Sex (female/male)	31/20	37/27	0.74	
AST (IU/L)	44.5 ± 42.6	64.6 ± 44.9	0.02	
ALT (IU/L)	53.0 ± 56.3	71.3 ± 55.5	0.08	
Platelets ($\times 10^9$/L)	186 ± 47	142 ± 50	<0.001	
LF index	2.60 ± 0.59	3.51 ± 0.84	<0.001	0.25 (0.11–0.55)

ALT, alanine aminotransferase; AST, aspartate aminotransferase; CI, confidence interval; LF, liver fibrosis.

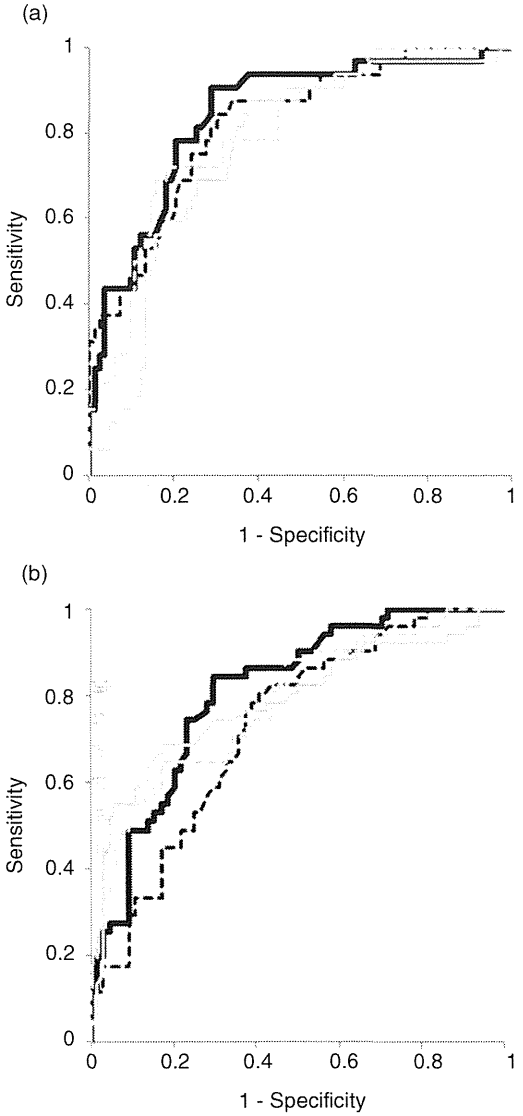

Figure 4 Receiver-operator curves (ROC) of liver fibrosis (LF) index and serum fibrosis markers. (a) ROC for diagnosis of significant fibrosis (F3–4). (b) ROC for diagnosis of minimal fibrosis (F0–1). —, LF index; ----, platelets; , aspartate aminotransferase-to-platelet ratio index; , FIB-4 index.

markers based on blood laboratory tests for predicting liver fibrosis.

Transient elastography has been most commonly used to measure liver stiffness and is established in clinical practice to evaluate liver fibrosis.[8,9] RTE exhibits some advantages compared with transient elastography. In this study, RTE imaging was successfully performed in all patients, and LF index was calculated. Although transient elastography has high diagnostic capabilities when it comes to liver fibrosis, measurements are sometimes impossible in patients with severe obesity and ascites.[24] Reproducibility of transient elastography was reportedly lower in patients with steatosis, inflammation, increased body mass index and lower degrees of liver fibrosis.[25–27] On the other hand, LF index is measured by ultrasound guidance that facilitates the identification of a suitable location for elastographic measurement, thereby resulting in a higher number of patients with valid results.

Unlike transient elastography, another advantage of LF index is that the results are not influenced by the presence of inflammation and steatosis. It was reported that LF index is not useful in patients with steatosis.[22] However, LF index was not significantly different between patients with and without steatosis in the present study even after stratification by fibrosis stage. Thus, LF index was useful for prediction of fibrosis in CHC patients regardless of steatosis. Because LF index of each activity grade and steatosis grade did not differ from each other, estimation of liver fibrosis by LF index demonstrated higher reproducibility than transient elastography.

In previously reports, diagnostic accuracy of liver fibrosis using RTE was inferior to transient elastography;[28] however, other studies have reported contrasting results.[19] The reason for this variability is probably because RTE technology and the equations used to calculate tissue elasticity are rapidly changing. The utility of elastic ratio, another RTE method for evaluation of liver fibrosis, was reported.[20] The elastic ratio is the ratio between the tissue compressibility of the liver and that of the intrahepatic small vessel. The AUROC of elastic ratio for predicting advanced fibrosis was 0.94 and was superior to LF index. Further, ARFI and real-time shear wave elastography were reported to have a high diagnostic accuracy of liver fibrosis.[10,11,29] There are currently no studies that directly compare LF index and those methods for diagnostic value of liver fibrosis. Therefore, further studies are needed to fully explore the potential of RTE, especially with regard to LF index.

Our study had several limitations. The number of patients with advanced fibrosis was small. The potential of LF index to differentiate patients with F3 and F4 needs to be explored with a large number of patients. Further, validation study is needed to evaluate the diagnostic accuracy of fibrosis stage, especially in comparison with other modalities.

In conclusion, LF index calculated by RTE is useful for predicting liver fibrosis, and diagnostic accuracy of LF index is superior to that of serum fibrosis markers.

Table 4 Diagnostic performance of LF index and serum fibrosis markers

	F0–2 vs F3–4					F0–1 vs F2–4				
	AUROC	Sensitivity (%)	Specificity (%)	PPV (%)	NPV (%)	AUROC	Sensitivity (%)	Specificity (%)	PPV (%)	NPV (%)
LF index	0.84	90.6	71.1	54.7	95.2	0.81	84.3	70.3	69.4	84.9
Platelets	0.82	87.5	66.3	50.0	93.2	0.73	80.4	59.4	61.2	79.2
FIB-4 index	0.80	71.9	81.9	60.5	88.3	0.79	54.9	90.6	82.3	71.6
APRI	0.76	87.5	61.4	46.7	92.7	0.78	64.7	85.9	78.6	75.3

APRI, aspartate aminotransferase/platelet ratio index; AUROC, area under the receiver–operator curve; NPV, negative predictive value; PPV, positive predictive value.

ACKNOWLEDGMENT

THIS STUDY WAS supported by a Grant-in-Aid from Ministry of Health, Labor, and Welfare, Japan.

REFERENCES

1 Serfaty L, Aumaitre H, Chazouilleres O *et al.* Determinants of outcome of compensated hepatitis C virus-related cirrhosis. *Hepatology* 1998; **27:** 1435–40.
2 Benvegnu L, Gios M, Boccato S, Alberti A. Natural history of compensated viral cirrhosis: a prospective study on the incidence and hierarchy of major complications. *Gut* 2004; **53:** 744–9.
3 Dienstag JL. The role of liver biopsy in chronic hepatitis C. *Hepatology* 2002; **36:** S152–60.
4 Gebo KA, Herlong HF, Torbenson MS *et al.* Role of liver biopsy in management of chronic hepatitis C: a systematic review. *Hepatology* 2002; **36:** S161–72.
5 Namiki I, Nishiguchi S, Hino K *et al.* Management of hepatitis C; Report of the Consensus Meeting at the 45th Annual Meeting of the Japan Society of Hepatology (2009). *Hepatol Res* 2010; **40:** 347–68.
6 Bedossa P, Dargere D, Paradis V. Sampling variability of liver fibrosis in chronic hepatitis C. *Hepatology* 2003; **38:** 1449–57.
7 Intraobserver and interobserver variations in liver biopsy interpretation in patients with chronic hepatitis C. The French METAVIR Cooperative Study Group. *Hepatology* 1994; **20:** 15–20.
8 Sandrin L, Fourquet B, Hasquenoph JM *et al.* Transient elastography: a new noninvasive method for assessment of hepatic fibrosis. *Ultrasound Med Biol* 2003; **29:** 1705–13.
9 Friedrich-Rust M, Ong MF, Martens S *et al.* Performance of transient elastography for the staging of liver fibrosis: a meta-analysis. *Gastroenterology* 2008; **134:** 960–74.
10 Friedrich-Rust M, Wunder K, Kriener S *et al.* Liver fibrosis in viral hepatitis: noninvasive assessment with acoustic radiation force impulse imaging versus transient elastography. *Radiology* 2009; **252:** 595–604.
11 Palmeri ML, Wang MH, Rouze NC *et al.* Noninvasive evaluation of hepatic fibrosis using acoustic radiation force-based shear stiffness in patients with nonalcoholic fatty liver disease. *J Hepatol* 2011; **55:** 666–72.
12 Williams AL, Hoofnagle JH. Ratio of serum aspartate to alanine aminotransferase in chronic hepatitis. Relationship to cirrhosis. *Gastroenterology* 1988; **95:** 734–9.
13 Wai CT, Greenson JK, Fontana RJ *et al.* A simple noninvasive index can predict both significant fibrosis and cirrhosis in patients with chronic hepatitis C. *Hepatology* 2003; **38:** 518–26.
14 Lin ZH, Xin YN, Dong QJ *et al.* Performance of the aspartate aminotransferase-to-platelet ratio index for the staging of hepatitis C-related fibrosis: an updated meta-analysis. *Hepatology* 2011; **53:** 726–36.
15 Sterling RK, Lissen E, Clumeck N *et al.* Development of a simple noninvasive index to predict significant fibrosis in patients with HIV/HCV coinfection. *Hepatology* 2006; **43:** 1317–25.
16 Vallet-Pichard A, Mallet V, Nalpas B *et al.* FIB-4: an inexpensive and accurate marker of fibrosis in HCV infection. comparison with liver biopsy and fibrotest. *Hepatology* 2007; **46:** 32–6.
17 Tamaki N, Kurosaki M, Tanaka K *et al.* Noninvasive estimation of fibrosis progression overtime using the FIB-4 index in chronic hepatitis C. *J Viral Hepat* 2013; **20:** 72–6.
18 Friedrich-Rust M, Ong MF, Herrmann E *et al.* Real-time elastography for noninvasive assessment of liver fibrosis in chronic viral hepatitis. *AJR Am J Roentgenol* 2007; **188:** 758–64.
19 Morikawa H, Fukuda K, Kobayashi S *et al.* Real-time tissue elastography as a tool for the noninvasive assessment of liver stiffness in patients with chronic hepatitis C. *J Gastroenterol* 2011; **46:** 350–8.
20 Koizumi Y, Hirooka M, Kisaka Y *et al.* Liver fibrosis in patients with chronic hepatitis C: noninvasive diagnosis by means of real-time tissue elastography – establishment of the method for measurement. *Radiology* 2011; **258:** 610–17.

21 Tatsumi C, Kudo M, Ueshima K *et al.* Non-invasive evaluation of hepatic fibrosis for type C chronic hepatitis. *Intervirology* 2010; **53:** 76–81.
22 Tomeno W, Yoneda M, Imajo K *et al.* Evaluation of the Liver Fibrosis Index calculated by using real-time tissue elastography for the non-invasive assessment of liver fibrosis in chronic liver diseases. *Hepatol Res* 2012; **12:** 12023.
23 Bedossa P, Poynard T. An algorithm for the grading of activity in chronic hepatitis C. The METAVIR Cooperative Study Group. *Hepatology* 1996; **24:** 289–93.
24 Castera L, Foucher J, Bernard PH *et al.* Pitfalls of liver stiffness measurement: a 5-year prospective study of 13,369 examinations. *Hepatology* 2010; **51:** 828–35.
25 Fraquelli M, Rigamonti C, Casazza G *et al.* Reproducibility of transient elastography in the evaluation of liver fibrosis in patients with chronic liver disease. *Gut* 2007; **56:** 968–73.
26 Arena U, Vizzutti F, Abraldes JG *et al.* Reliability of transient elastography for the diagnosis of advanced fibrosis in chronic hepatitis C. *Gut* 2008; **57:** 1288–93.
27 Rizzo L, Calvaruso V, Cacopardo B *et al.* Comparison of transient elastography and acoustic radiation force impulse for non-invasive staging of liver fibrosis in patients with chronic hepatitis C. *Am J Gastroenterol* 2011; **106:** 2112–20.
28 Colombo S, Buonocore M, Del Poggio A *et al.* Head-to-head comparison of transient elastography (TE), real-time tissue elastography (RTE), and acoustic radiation force impulse (ARFI) imaging in the diagnosis of liver fibrosis. *J Gastroenterol* 2012; **47:** 461–9.
29 Ferraioli G, Tinelli C, Dal Bello B, Zicchetti M, Filice G, Filice C. Accuracy of real-time shear wave elastography for assessing liver fibrosis in chronic hepatitis C: a pilot study. *Hepatology* 2012; **56:** 2125–33.

Diabetologia
DOI 10.1007/s00125-013-3149-9

ARTICLE

The effects of ezetimibe on non-alcoholic fatty liver disease and glucose metabolism: a randomised controlled trial

Yumie Takeshita · Toshinari Takamura · Masao Honda · Yuki Kita · Yoh Zen · Ken-ichiro Kato · Hirofumi Misu · Tsuguhito Ota · Mikiko Nakamura · Kazutoshi Yamada · Hajime Sunagozaka · Kuniaki Arai · Tatsuya Yamashita · Eishiro Mizukoshi · Shuichi Kaneko

Received: 11 October 2013 / Accepted: 15 November 2013

Abstract

Aims/hypothesis The cholesterol absorption inhibitor ezetimibe has been shown to ameliorate non-alcoholic fatty liver disease (NAFLD) pathology in a single-armed clinical study and in experimental animal models. In this study, we investigated the efficacy of ezetimibe on NAFLD pathology in an open-label randomised controlled clinical trial.

Methods We had planned to enrol 80 patients in the trial, as we had estimated that, with this sample size, the study would have 90% power. The study intervention and enrolment were discontinued because of the higher proportion of adverse events (significant elevation in HbA_{1c}) in the ezetimibe group than in the control group. Thirty-two patients with NAFLD were enrolled and randomised (allocation by computer program). Ezetimibe (10 mg/day) was given to 17 patients with NAFLD for 6 months. The primary endpoint was change in serum aminotransferase level. Secondary outcomes were change in liver histology (12 control and 16 ezetimibe patients), insulin sensitivity including a hyperinsulinaemic–euglycaemic clamp study (ten control and 13 ezetimibe patients) and hepatic fatty acid composition (six control and nine ezetimibe patients). Hepatic gene expression profiling was completed in 15 patients using an Affymetrix gene chip. Patients and the physician in charge knew to which group the patient had been allocated, but people carrying out measurements or examinations were blinded to group.

Results Serum total cholesterol was significantly decreased in the ezetimibe group. The fibrosis stage and ballooning score were also significantly improved with ezetimibe treatment. However, ezetimibe treatment significantly increased HbA_{1c} and was associated with a significant increase in hepatic long-chain fatty acids. Hepatic gene expression analysis showed coordinate downregulation of genes involved in skeletal muscle development and cell adhesion molecules in the ezetimibe treatment group, suggesting a suppression of stellate cell development into myofibroblasts. Genes involved in the L-carnitine pathway were coordinately downregulated by ezetimibe treatment and those in the steroid metabolism pathway upregulated, suggestive of impaired oxidation of long-chain fatty acids.

Conclusions/interpretation Ezetimibe improved hepatic fibrosis but increased hepatic long-chain fatty acids and HbA_{1c} in patients with NAFLD. These findings shed light on previously unrecognised actions of ezetimibe that should be examined further in future studies.

Trial registration University Hospital Medical Information Network (UMIN) Clinical Trials Registry UMIN000005250.

Funding The study was funded by grants-in-aid from the Ministry of Education, Culture, Sports, Science and Technology, Japan, and research grants from MSD.

Keywords Ezetimibe · Fatty acid · Gene expression · Non-alcoholic fatty liver disease

Yumie Takeshita and Toshinari Takamura contributed equally to this work.

Electronic supplementary material The online version of this article (doi:10.1007/s00125-013-3149-9) contains peer-reviewed but unedited supplementary material, which is available to authorised users.

Y. Takeshita · T. Takamura (✉) · M. Honda · Y. Kita · K.-i. Kato · H. Misu · T. Ota · M. Nakamura · K. Yamada · H. Sunagozaka · K. Arai · T. Yamashita · E. Mizukoshi · S. Kaneko
Department of Disease Control and Homeostasis, Kanazawa University Graduate School of Medical Sciences, 13-1 Takara-machi, Kanazawa, Ishikawa 920-8641, Japan
e-mail: ttakamura@m-kanazawa.jp

Y. Zen
Histopathology Section, Institute of Liver Studies, King's College Hospital, London, UK

Published online: 10 January 2014

Abbreviations

ALT	Alanine aminotransferase
H-IR	Hepatic insulin resistance index
hsCRP	High-sensitivity C-reactive protein
ICG15	Indocyanine green retention rate at 15 min after venous administration
LXR	Liver-X-receptor
MCR	Glucose metabolic clearance rate
miR	MicroRNA
NAFLD	Non-alcoholic fatty liver disease
NAS	NAFLD activity score
NASH	Non-alcoholic steatohepatitis
NPC1L1	Niemann–Pick C1-like 1
PAI-1	Plasminogen activator inhibitor-1
RLP-C	Remnant-like particle cholesterol
sdLDL	Small dense LDL
SREBP	Sterol regulatory element binding protein
QUICKI	Quantitative insulin sensitivity check index

Introduction

Multiple metabolic disorders, such as diabetes [1], insulin resistance and dyslipidaemia [2], are associated with non-alcoholic fatty liver disease (NAFLD), ranging from simple fatty liver to non-alcoholic steatohepatitis (NASH). Steatosis of the liver is closely associated with insulin resistance. However, the toxic lipids are not intrahepatic triacylglycerols but, rather, it is non-esterified cholesterol [3, 4] and some NEFA [5] that contribute to inflammation and insulin resistance in hepatocytes.

The level of cholesterol is tightly regulated by endogenous synthesis in the liver and dietary absorption/biliary reabsorption in the small intestine. Niemann–Pick C1-like 1 (NPC1L1) plays a pivotal role in cholesterol incorporation in enterocytes [6]. Ezetimibe, a potent inhibitor of cholesterol absorption, inhibits NPC1L1-dependent cholesterol transport at the brush border of the intestine and the liver [6]. This suggests that ezetimibe ameliorates toxic-lipid-induced inflammation and insulin resistance by inhibiting cholesterol absorption. Indeed, ezetimibe improves liver steatosis and insulin resistance in mice [7] and Zucker obese fatty rats [8], although the beneficial effects of ezetimibe are observed only when the animals are fed a high-fat diet. Ezetimibe can also ameliorate liver pathology in patients with NAFLD [9, 10]; however, these studies lack a control group, which precludes meaningful conclusions as liver pathology can improve over the natural course of the disease or with tight glycaemic control in some NAFLD patients [1]. In the present study, we investigated the efficacy of ezetimibe treatment in patients with NAFLD for 6 months in an open-label randomised control study by examining liver pathology, as well as hepatic enzymes, glucose metabolism, hepatic fatty acid composition and hepatic gene expression profiles.

Methods

Patient selection Study staff recruited participants from outpatients at Kanazawa University Hospital, Ishikawa, Japan. Patients were recruited from April 2008 to August 2010, with follow-up visits during the 6 months thereafter. The study lasted from April 2008 to February 2011.

The inclusion criterion was a biopsy consistent with the diagnosis of NAFLD. Exclusion criteria included hepatic virus infections (hepatitis C virus [HCV] RNA–PCR-positive, hepatitis B and C, cytomegalovirus and Epstein–Barr virus), autoimmune hepatitis, primary biliary cirrhosis, sclerosing cholangitis, haemochromatosis, α_1-antitrypsin deficiency, Wilson's disease, history of parenteral nutrition and use of drugs known to induce steatosis (e.g. valproate, amiodarone and prednisone) or hepatic injury caused by substance abuse and/or the current or past consumption of more than 20 g of alcohol daily. None of the patients had any clinical evidence of hepatic decompensation, such as hepatic encephalopathy, ascites, variceal bleeding or an elevated serum bilirubin level more than twofold the upper normal limit.

A random allocation sequence was computer-generated elsewhere and assigned participants in a 1:1 ratio to treatment with ezetimibe or to the control group. All patients and responsible guardians underwent an hour of nutritional counselling by an experienced dietitian before starting the 6 month treatment period. The experienced dietitians were unaware of the study assignments. In addition, all patients were given a standard energy diet (125.5 kJ/kg per day; carbohydrate 50–60%, fat 20–30%, protein 15–20%) and exercise (5–6 metabolic equivalent estimations for 30 min daily) counselling before the study. Patients remained on stable doses of medications for the duration of the study. The patients in the ezetimibe group received generic ezetimibe (10 mg/day; Zetia, [Merck, Whitehouse Station, NJ, USA]) for 6 months.

The study was conducted with the approval of the Ethics Committee of Kanazawa University Hospital, Ishikawa, Japan, in accordance with the Declaration of Helsinki. Written informed consent was obtained from all individuals before enrolment. This trial is registered with the University Hospital Medical Information Network (UMIN) (Clinical Trials Registry, no. UMIN000005250).

Primary and secondary outcomes The primary endpoint was change in serum alanine aminotransferase (ALT) level at month 6 from baseline. Secondary outcomes included changes in the histological findings for NAFLD, hepatic gene expression profiling, fatty acid compositions of plasma and liver biopsy samples, lipid profiles, insulin resistance and

anthropometric measures, as well as assessment of ezetimibe safety. We had planned to enrol 80 patients in the trial, as we had estimated that with this sample size, the study would have 90% power at an α (two-tailed) value of 0.05 showing a 50% decrease of serum ALT values with 6 months of pioglitazone therapy on the basis of a previous study [11]. At the time of adverse event analyses, 32 of the targeted 80 patients had been randomly assigned and were included in the safety analyses.

Data collection Clinical information, including age, sex and body measurements, was obtained for each patient. Venous blood samples were obtained after the patients had fasted overnight (12 h) and were used to evaluate blood chemistry. Insulin resistance was estimated by HOMA-IR, calculated as [fasting insulin (pmol/l) × fasting glucose (mmol/l)]/22.5 [12] and insulin sensitivity was estimated as the quantitative insulin sensitivity check index (QUICKI)[13]. The adipose tissue insulin resistance index (adipose IR) was calculated as fasting NEFA (mmol/l)×fasting insulin (pmol/l) [14–16]. The indocyanine green retention rate at 15 min after venous administration (ICG15) was assessed using standard laboratory techniques before and after treatment. Serum fatty acids were measured with a gas chromatograph (Shimizu GC 17A, Kypto, Japan) at SRL (Tokyo, Japan).

Evaluation of insulin sensitivity derived from an OGTT After an overnight fast (10–12 h), a 75 g OGTT was performed at 08:30 hours. The OGTT-derived index of beta cell function, the insulinogenic index, computed as the suprabasal serum insulin increment divided by the corresponding plasma glucose increment in the first 30 min (ΔI30/ΔG30) [15, 17, 18] was calculated. From the OGTT data, the Matsuda index [19] was calculated. The hepatic insulin resistance index (H-IR) was calculated as the product of the total AUCs for glucose and insulin during the first 30 min of the OGTT (glucose 0–30 [AUC] [mmol/l]×insulin 0–30 [AUC] [pmol/l]). Skeletal muscle insulin sensitivity can be calculated as the rate of decline in plasma glucose concentration divided by plasma insulin concentration, as follows. Muscle insulin sensitivity index=dG/dt/mean plasma insulin concentration, where dG/dt is the rate of decline in plasma glucose concentration and is calculated as the slope of the least square fit to the decline in plasma glucose concentration from peak to nadir [20]. See the electronic supplementary material (ESM) for further details.

Evaluation of insulin sensitivity derived from the euglycaemic insulin clamp Insulin sensitivity in 23 of the 31 patients (10 control and 13 ezetimibe patients) was also evaluated in a hyperinsulinaemic–euglycaemic clamp study [21]. Patients did not receive any medication on the morning of the examination. At ~09:00 hours, after an overnight fast of at least 10 h, an intravenous catheter was placed in an antecubital vein in each individual for infusion, while a second catheter was placed in the contralateral hand for blood sampling. The euglycaemic–hyperinsulinaemic clamp technique was performed using an artificial pancreas (model STG-22; Nikkiso, Tokyo, Japan), as described previously [22]. See ESM for further details. The mean glucose metabolic clearance rate (MCR) in healthy individuals (n=9; age, 26.60± 2.9 years; body mass index, 22.3±2.1 kg/m^2) was 13.5± 3.4 mg kg^{-1} min^{-1} [2].

Liver biopsy pathology A single pathologist, who was blinded to the clinical information and the order in which the biopsies were obtained, analysed all biopsies twice and at separate times. The sections were cut from a paraffin block and stained with haematoxylin and eosin, Azan–Mallory and silver reticulin impregnation. The biopsied tissues were scored for steatosis (from 0 to 3), stage (from 1 to 4) and grade (from 1 to 3) as described [2], according to the standard criteria for grading and staging of NASH proposed by Brunt et al [23]. The NAFLD activity score (NAS) was calculated as the unweighted sum of the scores for steatosis (0–3), lobular inflammation (0–3) and ballooning (0–2), as reported by Kleiner et al [24].

Gene expression analysis of liver biopsied samples Gene expression profiling was performed in samples from nine patients in the ezetimibe group and six in the control group. Liver tissue RNA was isolated using the RNeasy Mini kit (QIAGEN, Tokyo, Japan) according to the manufacturer's instructions. See ESM for further details. Data files (CEL) were obtained using the GeneChip Operating Software 1.4 (Affymetrix). Genechip data analysis was performed using BRB-Array Tools (http://linus.nci.nih.gov/BRB-ArrayTools.html). The data were log-transformed ($\log_{10}$), normalised and centred. To identify genetic variants, paired t tests were performed to define p values <0.05 and fold change>1.5. Pathway analysis was performed using MetaCore (GeneGo, St Joseph, MI, USA). Functional ontology enrichment analysis was performed to compare the gene ontology (GO) process distribution of differentially expressed genes ($p < 0.01$).

Fatty acid composition of liver Aliquots (0.2 mg) of liver samples snap-frozen by liquid nitrogen were homogenised in 1 ml normal NaCl solution (NaCl 154 mmol/l). Briefly, fatty acids were extracted by using pentadecanoic acid, and saponified with alkaline reagent (0.5 mmol/l KOH/ CH_3OH). The fatty acid methyl esters were analysed in a gas chromatograph (Shimadzu GC-2014 AF/SPL; Shimadzu Corporation, Kyoto, Japan) equipped with a flame ionisation detector and an auto injector. See ESM for further details. Mass spectra were analysed using GC solution (v. 2.3) software (Shimadzu Corporation, Kyoto, Japan, www.shimadzu.com). The changes in hepatic fatty acid composition are expressed as 10^{-4} mg/mg liver.